

Fractality of deterministic diffusion in the nonhyperbolic climbing sine map

N. Korabel and R. Klages

Max-Planck-Institut für Physik komplexer Systeme, Nöthnitzer Straße 38, D-01187 Dresden, Germany

Abstract

The nonlinear climbing sine map is a nonhyperbolic dynamical system exhibiting both normal and anomalous diffusion under variation of a control parameter. We show that on a suitable coarse scale this map generates an oscillating parameter-dependent diffusion coefficient, similarly to hyperbolic maps, whose asymptotic functional form can be understood in terms of simple random walk approximations. On finer scales we find fractal hierarchies of normal and anomalous diffusive regions as functions of the control parameter. By using a Green-Kubo formula for diffusion the origin of these different regions is systematically traced back to strong dynamical correlations. Starting from the equations of motion of the map these correlations are formulated in terms of fractal generalized Takagi functions obeying generalized de Rham-type functional recursion relations. We finally analyze the measure of the normal and anomalous diffusive regions in the parameter space showing that in both cases it is positive, and that for normal diffusion it increases by increasing the parameter value.

Key words: Deterministic diffusion, nonhyperbolic maps, fractal diffusion coefficient, anomalous diffusion, periodic windows

PACS: 05.45.Df, 05.10.-a, 05.45.Ac, 05.60.-k

1 Introduction

Low-dimensional time-discrete maps are among the most important models for exploring different aspects of chaos. These systems display a very rich dynamical behavior but are still very amenable to straightforward computer simulations. Even more, in some cases rigorous analytical solutions are possible. After it was realized that diffusion processes can be generated by microscopic deterministic chaos in the equations of motion, time-discrete maps became useful

tools in deterministic transport theory. The analysis of these simple models required to suitably combine nonequilibrium statistical mechanics with dynamical systems theory leading to a more profound understanding of transport in nonequilibrium situations [1,2,3,4]. However, time-discrete maps provide not only a suitable starting point for studying normal diffusion but also for investigating the anomalous case [5,6,7,8,9,10,11,12,13,14,15,16,17,18,19,20,21,22,23,24,25,26]. Moreover, there are certain classes of more realistic models which share specific properties of maps such as being low-dimensional and exhibiting certain periodicities. Indeed, theoretical investigations of chaotic billiards subject to external fields [27], of periodic Lorentz gases [28,29], and of pendulum-like differential equations [30,31,32,33,34,35,36] showed that many properties of deterministic transport in maps carry over to these more complex chaotic dynamical systems.

In this framework, recently a new feature of deterministic diffusion was discovered. For simple one-dimensional hyperbolic maps it was shown that the diffusion coefficient is typically a fractal function of control parameters [37,38,39,40]. Subsequently an analogous behavior was detected for other transport coefficients [41,42], and in more complicated models [27,28,29]. However, up to now the fractality of transport coefficients could be assessed for hyperbolic systems only, whereas, to our knowledge, the fractal nature of classical transport coefficients in the broad class of nonhyperbolic systems was not discussed.

On the other hand, studying nonhyperbolic dynamics appears to be more relevant in order to connect fractal transport coefficients to some known experiments. Here we think particularly of dissipative systems driven by periodic forces such as Josephson junctions in the presence of microwave radiation [43,44,45,46,47,48,49], superionic conductors [50,51], and systems exhibiting charge-density waves [52] in which certain features of deterministic diffusion were already observed experimentally. For these systems the equations of motion are typically of the form of some nonlinear pendulum equation. In the limiting case of strong dissipation they can be reduced to nonhyperbolic one-dimensional time-discrete maps sharing certain symmetries [53,54]. The so-called climbing sine map is a well-known example of this class of maps [5,6,9].

In this paper we pursue a detailed analysis of the diffusive and dynamical properties of the climbing sine map. Particularly, we show that the nonhyperbolicity of this map does not destroy the fractal characteristics of deterministic diffusive transport as they were found in hyperbolic systems. On the contrary, fractal structures appear for normal diffusive parameters as well as for anomalous diffusive regions. We argue that higher-order memory effects are crucial to understand the origin of these fractal hierarchies in this nonhyperbolic system. By using a Green-Kubo formula for diffusion, the dynamical correlations are recovered in terms of fractal Takagi-like functions. These functions appear as solutions of a generalized integro-differential de Rham-type equation. We fur-

thermore show that the distribution of periodic windows exhibiting anomalous diffusion forms Devil’s staircase like structures as a function of the parameter and that the complementary sets of chaotic dynamics have a positive measure in parameter space that increases by increasing the parameter value.

Our paper is organized as follows. In Sec. II we introduce the model. In Sec. III we explore the coarse functional form of the parameter-dependent diffusion coefficient and discuss it in relation to previous results on hyperbolic maps. In Sec. IV our analysis is refined revealing complex scenarios of anomalous diffusion, which are explained in terms of correlated random walk approximations. In Sec. V generalized fractal Takagi functions are constructed for the climbing sine map and the connection to the diffusion coefficient is worked out. Periodic windows exhibiting anomalous diffusion are studied in detail in Sec. VI. We then draw conclusions and discuss our results in the final section.

2 The climbing sine map

The one-dimensional climbing sine map is defined as

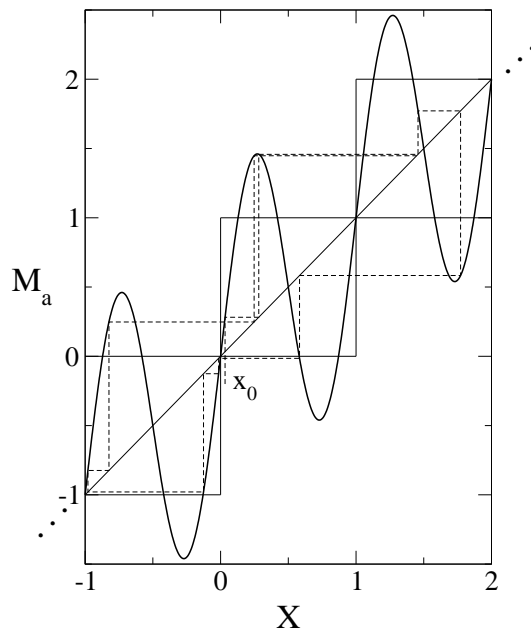


Fig. 1. Illustration of the climbing sine map for the particular parameter value of $a = 1.189$. The dashed line indicates the orbit of a moving particle starting from the initial position x_0 .

$$X_{n+1} = M_a(X_n), \quad M_a(X) = X + a \sin(2\pi X), \quad (1)$$

where $a \in \mathbb{R}$ is a control parameter and X_n is the position of a point particle at discrete time n . Obviously, $M_a(X)$ possesses translation and reflection

symmetry,

$$M_a(X + p) = M_a(X) + p, \quad M_a(-X) = -M_a(X). \quad (2)$$

The periodicity of the map naturally splits the phase space into different boxes, $(p, p + 1]$, $p \in \mathbb{Z}$, as shown in Fig. 1. Eq. (1) as restricted to one box, i.e., on a circle, we call the reduced map,

$$m_a(x) := M_a(X) \bmod 1, \quad x := X \bmod 1. \quad (3)$$

The probability $\rho_n(x)dx$ to find a particle at a position between x and $x + dx$ at time n then evolves according to the continuity equation for the probability density $\rho_n(x)$, which is the Frobenius-Perron equation [55]

$$\rho_{n+1}(x) = \int dy \rho_n(y) \delta(x - m_a(y)). \quad (4)$$

The stationary solution of this equation is called the invariant density, which we denote by $\rho^*(x)$.

Due to its nonhyperbolicity, the climbing sine map possesses a rich dynamics consisting of chaotic diffusive motion, ballistic dynamics, and localized orbits. Under parameter variation these different types of dynamics are highly intertwined resulting in complicated scenarios related to the appearance of periodic windows [6,9]. In order to study diffusion we will be interested in parameters that are greater than $a > a_0 = 0.732644\dots$ for which the extrema of the map exceed the boundaries of each box for the first time indicating the onset of diffusive motion.

3 Coarse structure of the parameter-dependent diffusion coefficient

In this section we explore the relationship between nonlinear maps like the climbing sine map and simple piecewise linear maps for which, in contrast to the climbing sine map, the diffusion coefficient can be calculated exactly. It is well-known that in special cases such different types of maps are linked to each other via the concept of conjugacy. Indeed, we show that maps which are approximately conjugate to each other exhibit a very similar oscillatory behavior in the diffusion coefficient on coarse scales. Our argument refers to some existing methods for calculating the diffusion coefficient of piecewise linear maps, which we briefly review. We then describe how we numerically calculated the complete parameter dependence of the diffusion coefficient for the climbing sine map and discuss a first result.

3.1 *Computing and comparing the diffusion coefficient for approximately conjugate maps*

One speaks of normal deterministic diffusion if the mean square displacement of an ensemble of moving particles grows linearly in time. The diffusion coefficient is then given by the Einstein relation

$$D(a) = \lim_{n \rightarrow \infty} \langle X_n^2 \rangle / (2n), \quad (5)$$

where the brackets denote an ensemble average over the moving particles.

There exist various efficient numerical as well as, for some system parameters, analytical methods to exactly compute diffusion coefficients for piecewise linear hyperbolic maps, such as transition matrix methods based on Markov partitions [37,38,39,40], cycle expansion methods [15,16,17,18], and more recently a very powerful method related to kneading sequences [42].

We first restrict our analysis of diffusion in the climbing sine map to parameters for which there are simple Markov partitions. For one-dimensional maps, a partition is a Markov partition if and only if parts of the partition get mapped again onto parts of the partition, or onto unions of parts of the partition, see Ref. [38] and further references therein. An example of a Markov partition consisting of five parts is shown in the inset of Fig. 2. In case of the climbing sine map Markov partitions can be constructed simply by forward iteration of one of the critical points x_c defined by the condition that $m'_a(x_c) \equiv 0$ in the reduced map. If higher iterations of this point fall onto a periodic orbit a Markov partition exists. Indeed, if a Markov partition is known, for piecewise linear maps the diffusion coefficient can often be calculated analytically via calculating the invariant measure of the map or via computing the second largest eigenvalue of the Frobenius-Perron operator written in form of a transition matrix.

One can now identify an infinite series of parameter values corresponding to a certain type of Markov partition [37,38,39,40]. For parameter values which belong to such a Markov partition series the corresponding invariant densities $\rho^*(x)$ have a very similar functional form. Note that, in case of nonlinear maps, singularities in the invariant density exactly correspond to the iteration of the critical point x_c [56]. An example of $\rho^*(x)$ for one series of parameter values (marked as filled circles) is shown in the inset of Fig. 2.

By using respective series of Markov partitions piecewise linear maps can be related to nonlinear maps. For this purpose let us consider, along with the

climbing sine map, (i) the piecewise linear zig-zag map [7,8,16,17]

$$M_a(x_n) = \begin{cases} m_1 x_n, & 0 \leq x_n < b_1 \\ -m_2(x_n - b_1) + a, & b_1 \leq x_n < b_2 \\ m_1(x_n - 1) + 1, & b_2 \leq x_n < 1 \end{cases} \quad (6)$$

with $m_1 = m_2 = 4a - 1$, $b_1 + b_2 = 1$ and $b_1 = a/m_1$, and (ii) the nonlinear cubic map [6,55]

$$M_a(x_n) = ax_n^3 - \frac{3}{2}ax_n^2 + x_n(1 + \frac{1}{2}a). \quad (7)$$

The definitions of both maps are given on the unit interval.

In order to compare the diffusion coefficient of these different maps, the parameters a were chosen such that the maps all display the same height h , defined as the distance between the first iteration of the leftmost critical point $m_a(x_c)$ and the zero bound in the first box $(0, 1]$. Thus, $h = 1$ corresponds to the onset of diffusion for all three maps.

For the two simple Markov partition series $m_a(x_c) = 0$ and $m_a(x_c) = 0.5$, corresponding to integer and half-integer values of h , respectively, the diffusion coefficient of the zig-zag map can be calculated analytically. For integer values of h the result reads [8,16]

$$D(h) = \frac{h(h-1)(2h-1)}{3(4h-1)}. \quad (8)$$

For half-integer values of h the diffusion coefficient is easily calculated analytically, e.g., by transition matrix methods [38,40], to

$$D(h) = \frac{h(4h^2-1)}{6(4h-1)}. \quad (9)$$

In case of the climbing sine map and of the cubic map the diffusion coefficient was obtained from computer simulations by evaluating the mean square displacement Eq. (5) for the same series of Markov partitions. Results are shown in Fig. 2. For the climbing sine map some more Markov partition series points (altogether five different series) were included. For all three maps there is a very analogous oscillatory behavior of the parameter-dependent diffusion coefficient. These oscillations can be explained in terms of the changes of the microscopic dynamics under parameter variation, that is, whenever there is a local maximum there is an onset of strong backscattering in the dynamics yielding a local decrease of the diffusion coefficient in the parameter, and vice versa at local minima [37,38,39,40]. However, the five Markov partition series for the climbing sine diffusion coefficient already indicate that there are more irregularities on finer scales. For piecewise linear maps, the origin of these

irregularities was identified to be the topological instability of the dynamics under parameter variation [38,40]. That is, a small deviation of the parameter changes the Markov partition and the corresponding invariant density which, in turn, is reflected in a change of the value of the diffusion coefficient. Note that the dependence of the diffusion coefficient for a single Markov partition series appears to be a monotonously increasing function of the parameter [57]. Nevertheless, computing $D(a)$ for more and more Markov partitions series will reveal more and more irregularities in $D(a)$ thus forming a fractal structure [37,38,39,40].

Since the climbing sine map shares the same topological features as piecewise linear maps in terms of these series of Markov partitions, one may wonder whether it is not possible to straightforwardly calculate the diffusion coefficient for nonlinear maps from the one of piecewise linear maps by using the concept of conjugacy [9,55,58], see also the definition in Appendix A. In fact, it was stated by Grossmann and Thomae [9] that the diffusion coefficient is invariant under conjugacy, however, without giving a proof. In Appendix A such a proof is provided. Unfortunately, conjugacies are explicitly known only in very specific cases and for maps acting on the unit interval [55,58]. As soon as the map extrema exceed the unit interval, which is reminiscent of the onset of diffusive behavior, only some approximate, piecewise conjugacies could be constructed in a straightforward way, see Ref. [9] for an example.

We now apply this reasoning along the lines of conjugacy in order to understand the similarities between the diffusion coefficient of the three maps as displayed in Fig. 2. The functional form of the cubic map can be obtained from a Taylor series expansion of $\sin(x_n)$ by keeping terms up to third order thus representing a low-order approximation of the climbing sine map. This seems to be reflected in the fact that at any odd integer parameter value of h the climbing sine map has an invariant density whose functional form is very close to the one of the cubic map at parameter value $h = 1$, $\rho^*(x) = \pi^{-1}(x(1-x))^{-1/2}$. Hence, one may expect that both diffusion coefficients are possibly trivially related to each other, however, note the increasing deviations between the respective results at larger h .

For $h = 1$, the cubic map and the piecewise linear zig-zag map are now in turn conjugate to each other [55,58]. However, for $h > 1$ we are not aware of the existence of any exact conjugacy between zig-zag and cubic map. Still, along the lines of Ref. [9] one can at least approximately relate both maps to each other via using piecewise conjugacies. This explains why the zig-zag map and the climbing sine map display qualitatively the very same oscillatory behavior in the diffusion coefficient, somewhat linked by diffusion in the cubic map.

In summary, by using Markov partitions and by arguing with the concept of conjugacy we have shown that the structure of the diffusion coefficient for the

nonlinear climbing sine map has much in common with the one of respective piecewise linear maps, in the sense of displaying a non-trivial oscillatory parameter dependence. However, to use conjugacies in order to exactly calculate the diffusion coefficient for nonlinear maps does not appear to be straightforward [56], hence in the following we restrict ourselves to alternative methods as discussed in the next subsection.

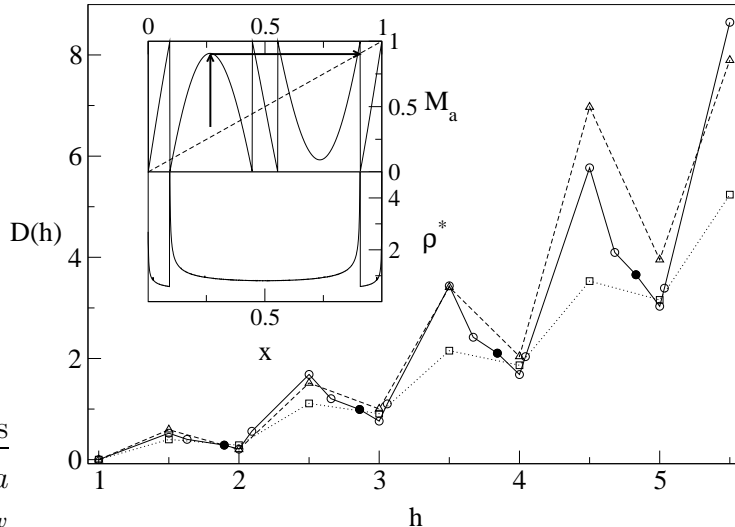


Fig. 2. Diffusion coefficient at certain Markov partition parameter values for three different maps, which are the zig-zag map Eq.(6) (squares), the climbing sine map (circles), and the cubic map Eq. (7) (triangles). The values for the zig-zag map represent analytical results, see Eqs.(8,9), the remaining values are from computer simulations. The lines are guides for the eyes. The inset shows an example of a Markov partition for the climbing sine map on the unit interval and the corresponding invariant density.

3.2 Complete parameter dependence of the climbing sine diffusion coefficient

In order to obtain the full parameter dependence for the diffusion coefficient of the climbing sine map we numerically evaluated the Green-Kubo formula for diffusion in maps [3,4,8,29,38,41] reading

$$D_n(a) = \langle j_a(x) J_a^n(x) \rangle - \frac{1}{2} \langle j_a^2(x) \rangle. \quad (10)$$

Here the angular brackets denote an average over the invariant density of the reduced map, $\langle \dots \rangle = \int dx \rho^*(x) \dots$. The jump velocity $j_a(x)$ is defined by

$$j_a(x_n) := [X_{n+1}] - [X_n] \equiv [M_a(x_n)], \quad (11)$$

where the square brackets denote the largest integer less than the argument. The sum

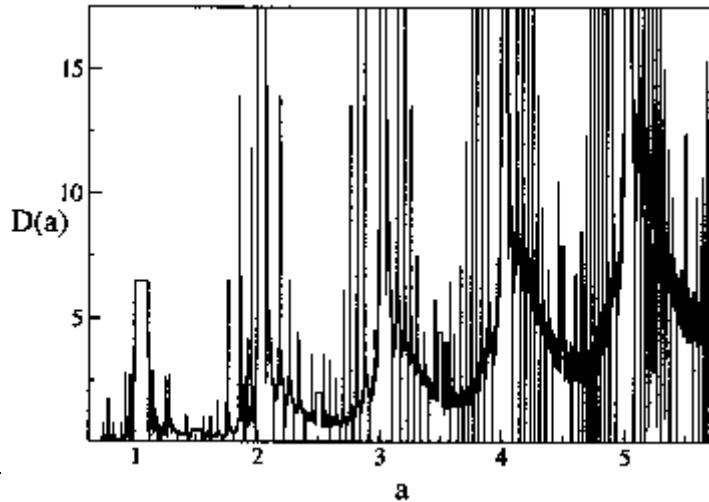


Fig. 3. Diffusion coefficient for the climbing sine map over a large range of parameter values. Note the oscillations on large and small scales. The small scale fluctuations represent regions of anomalous diffusion where the diffusion coefficient either diverges or vanishes. Some of the divergent regions are cut off after a certain number of iterations showing plateaus instead of singularities. The data set consists of 265005 points.

$$J_a^n(x) = \sum_{k=0}^n j_a(x_k) \quad (12)$$

gives the integer value of the displacement of a particle after n time steps that started at some initial position x , and we call it jump velocity function. Eq. (10) defines a time-dependent diffusion coefficient which, in case of normal diffusion, converges to

$$D(a) = \lim_{n \rightarrow \infty} D_n(a). \quad (13)$$

In our simulations for Fig. 3 we truncated $J_a^n(x)$ after 7 time steps. The invariant density was obtained by solving the continuity equation for $\rho^*(x)$ Eq. (4) with the histogram method of Ref. [1]. Note that both the integer displacement and the density are coupled via Eq. (10). Results for $D(a)$ are shown in Fig. 3 for a large range of parameters demonstrating a highly non-trivial behavior of the diffusion coefficient. The large-scale oscillations as predicted from the simple Markov partition series (see Fig. 2) are still clearly seen, however, on top of this there exist further oscillations on finer scales. These are regions of anomalous diffusion that manifest themselves in form of abrupt divergences, $D(a) \rightarrow \infty$, or by a vanishing diffusion coefficient, $D(a) \rightarrow 0$.

4 Simple and correlated random walk approximations

In this section we study the parameter-dependent diffusion coefficient in more detail. Based on the Green-Kubo formula we derive a systematic hierarchy of approximations for the diffusion coefficient and show how they can be used to understand the complex behavior of this curve in more detail.

4.1 Asymptotic functional form of the diffusion coefficient on large scales

We are first interested in understanding the coarse functional form of the parameter-dependent diffusion coefficient in the limit of very small and very large parameter values. For this purpose we use simple random walk approximations that are based on the assumption of a complete loss of memory between the single jumps. Such an analysis was already performed for hyperbolic piecewise linear maps [38,39]. Here we apply the same reasoning to the nonlinear case of the climbing sine map.

We start in the limit of very small parameter values, i.e., near the onset of diffusion. Here we assume that particles make either a step of length one to the left or to the right, or just remain in the box. The transition probability is then given by integrating over the respective invariant density in the escape region. Putting all this information into Eq. (5) yields [6]

$$D(a) \simeq \rho(x_c)(2\epsilon/a_0\pi^2)^{1/2}, \quad (14)$$

where $\epsilon = a - a_0$. Making the additional approximation that $\rho(x) \simeq 1$ we get

$$D(a) \simeq 0.525\epsilon^{1/2}, \quad \epsilon \ll 1. \quad (15)$$

The other limiting case concerns values of $a \gg 1$. Here the precise value of the width of the escape region is much less important than the precise value of the step length which is very large, hence by again assuming that $\rho(x) \simeq 1$ Eq. (5) can be approximated to [38,39]

$$D(a) \approx \frac{1}{2} \int_0^1 dx (M_a(x) - x)^2 \approx \frac{a^2}{4}, \quad a \gg 1. \quad (16)$$

These two asymptotic random walk approximations are shown in Fig. 4 as bold lines. One can clearly see that there is a dynamical crossover between the different functional forms of these two asymptotic regimes. This crossover was first observed in piecewise linear maps and appears to be typical for diffusive systems exhibiting some spatial periodicity [38,39]. It was later on also verified for diffusion in the periodic Lorentz gas [28]. The coarse functional form of the

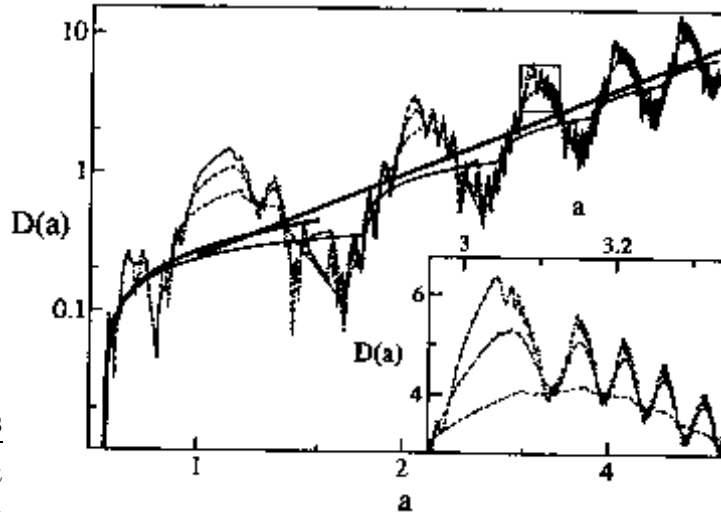


Fig. 4. Dynamical crossover in the climbing sine map. The two asymptotic regimes at small and large parameter values are approximated by simple random walk arguments yielding the functional forms shown as bold lines. The series of more irregular curves corresponds to higher-order correlated random walk approximations with $n = 0, 1, 2, 3$, which give an indication of the exact functional form. The magnification (inset in normal scale) of a small region around $a = 3$ shows more irregularities on a finer scale pointing towards a fractal structure of the diffusion coefficient.

random walk approximations should be compared to a certain series of higher-order approximations based on the Green-Kubo formula Eq. (10), which is also shown in the figure. These refined approximations are getting closer and closer to the exact functional form, as explained below, and thus give a good indication for these exact values.

4.2 Fine scale of the diffusion coefficient: anomalous diffusion and bifurcations

In the previous subsection we have outlined two simple random walk approximations for diffusion that do not include any memory effects. However, one can do better by systematically evaluating the single terms as contained in the series expansion of the Green-Kubo formula Eqs. (10,12). For a simple piecewise linear map and for the periodic Lorentz gas this was done in Ref. [29] and provided a simple approach to understand the origin of complex structures in the diffusion coefficient on fine scales.

The basic idea of this approach is as follows: The Green-Kubo formula Eq. (10) splits the dynamics into an inter-box dynamics, in terms of integer jumps, and into an intra-box dynamics, as represented by the invariant density. We first approximate the invariant density in Eq. (10) to $\rho(\tilde{x}) \simeq 1$ irrespective of the fact that it is typically a very complicated function of x and a [6,38].

The resulting approximate diffusion coefficient we label with a superscript in Eq. (10), $D_n^1(a)$. The term for $n = 0$ obviously excludes any higher-order correlations and was already worked out in form of the simple random walk approximation Eqs. (14)-(16).

The generalization $D_n^1(a)$, $n > 0$, which systematically includes more and more dynamical correlations, may consequently be denoted as *correlated random walk approximation* [29]. We now use this expansion to analyze the parameter dependence of the diffusion coefficient of the climbing sine map in terms of such higher-order correlations. Fig. 4 depicts results for $D_n(a)$ at

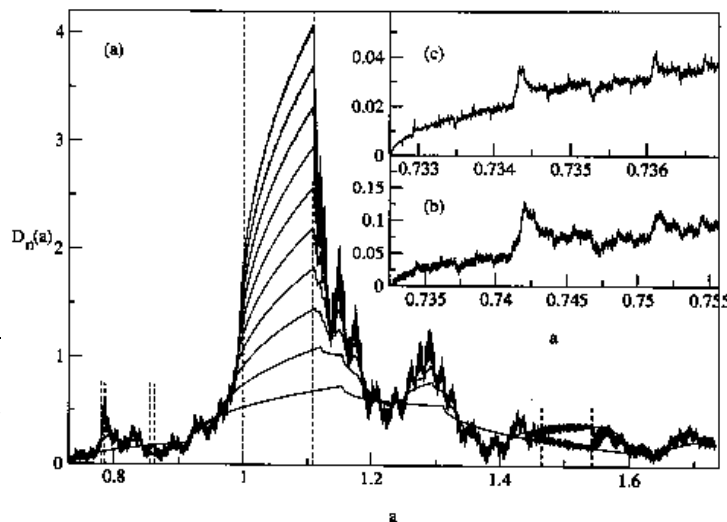


Fig. 5. (a) Sequence of correlated random walks $D_n^1(a)$, see Eq. (10) with uniform invariant density $\rho(x) \simeq 1$, for $n = 1, \dots, 10$. Note the quick convergence for normal diffusive parameters. The dashed lines define periodic windows, which are the same as in Fig.6. The insets (b) and (c) contain two magnifications of (a) in the region close to the onset of diffusion for $D_{10}^1(a)$ only. They show self-similar behavior on smaller and smaller scales.

$n = 0, 1, 2, 3$ over a large range of parameters, whereas Fig. 5 (a) presents a respective detailed analysis for the region close to the onset of diffusion, i.e., for parameters $a \in (0.732644, 1.742726]$, showing results for $D_n(a)$ at $n = 1, \dots, 10$. The series of approximations in Fig. 4 clearly reveals finer and finer sequences of oscillations that eventually converge to a fractal structure, as is particularly shown in the inset of this figure. However, here the order of the expansion is not large enough to identify parameter regions of anomalous diffusion. These regions can be better seen in Fig. 5, where three different cases of parameter regions can be distinguished: (i) regions with quick convergence of this approximation corresponding to normal diffusion (ii) divergence of $D_n^1(a)$ corresponding to ballistic motion, in agreement with $D(a) \rightarrow \infty$, and (iii) localized dynamics where $D_n^1(a)$ alternates in n between two solutions, with $D(a) \rightarrow 0$ for the exact diffusion coefficient. This oscillation points to the dynamical origin of localization in terms of certain period-two orbits. That

these approximate solutions are non-zero is due to the fact that the invariant density was set equal to one. The dashed lines in Fig. 5 indicate the largest regions of anomalous diffusion. The approximate diffusion coefficient $D_{10}^1(a)$ of this figure is compared to the “numerically exact” one in Fig. 6. Here “numerically exact” we wish to be understood in the sense that no further ad hoc-approximations are involved, i.e., we evaluated the Green-Kubo formula according to the numerical method described in Sec. III. by truncating it after 20 time steps. This comparison shows that in case of normal diffusion our approximation nicely reproduces the irregularities in the non-approximated diffusion coefficient. Like the inset of Fig. 4, the magnifications in Fig.5 give clear evidence for a self-similar structure of the diffusion coefficient. These results thus show that dealing with correlated jumps only yields a qualitative and to quite some extent even quantitative understanding of the regions of normal and anomalous diffusion in the climbing sine map.

The impact of specific features of the microscopic dynamics on the diffusion coefficient is nicely elucidated by comparing the bifurcation diagram of the reduced climbing sine map Eq. (3) with the numerically exact diffusion coefficient, see Fig. 6. As one can see in the upper panel of Fig. 6, the bifurcation diagram consists of (infinitely) many periodic windows. Whenever there is a window the dynamics of Eq. (1) is either ballistic or localized [6,8]. Fig. 6 demonstrates the strong impact of this bifurcation scenario on the diffusion coefficient. For localized dynamics, orbits are confined within some finite interval in phase space implying subdiffusive behavior for which the diffusion coefficient vanishes, whereas for ballistic motion particles propagate superdiffusively with a diverging diffusion coefficient being proportional to n . Only for normal diffusion $D(a)$ is nonzero, finite and the limit in Eq. (13) exists. At the boundaries of each periodic window the diffusion coefficient is related to intermittent-like transient behavior eventually resulting in normal diffusion with $D(a) \sim a^{(\pm\frac{1}{2})}$ [5,6,9,10].

5 Diffusion coefficient in terms of fractal generalized Takagi functions

In this section we further analyze the dynamical origin of the different structures in the parameter-dependent diffusion coefficient by constructing objects called fractal generalized Takagi functions. These functions somewhat resemble usual Takagi functions but, as will be shown, they fulfill a more complicated type of functional recursion relations than standard de Rham-type equations. Interestingly, Takagi functions were known to mathematicians since about a hundred years [59,60,61], however, in the field of chaotic transport they were appreciated by physicists only very recently [3,4,38,62,63].

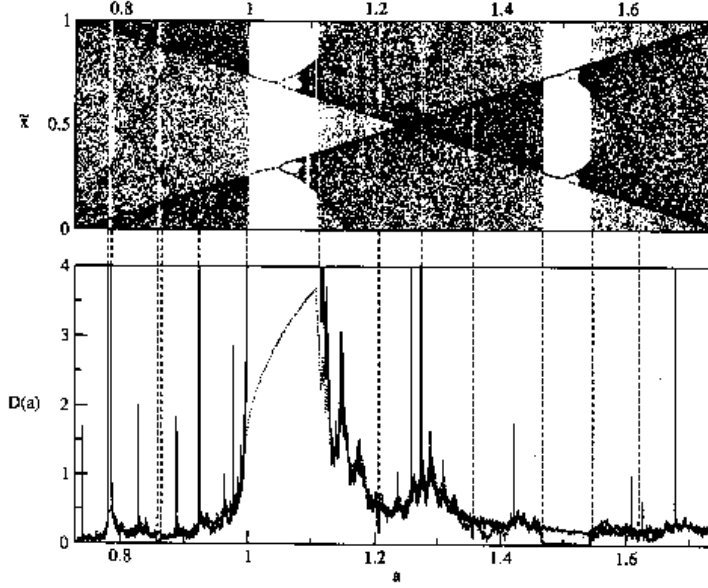


Fig. 6. Upper panel: bifurcation diagram for the climbing sine map. Lower panel: diffusion coefficient computed from simulations as a function of the control parameter a in comparison with the correlated random walk approximation $D_{10}^1(a)$ (dots). The dashed vertical lines connect regions of anomalous diffusion, $D(a) \rightarrow \infty$ or $D(a) \rightarrow 0$, with 'ballistic' and 'localized' windows, respectively, of the bifurcation diagram.

We first show how to construct fractal generalized Takagi functions and study their properties with respect to the three different types of dynamics in the climbing sine map. We then relate these objects directly to the diffusion coefficient.

From the definition of the time-dependent jump velocity function there follows the recursion relation [37,38]

$$J_a^n(x) = j_a(x) + J_a^{n-1}(m_a(x)). \quad (17)$$

Since the time-dependent jump velocity function J_a^n is getting extremely complicated after some time steps, we introduce the more well-behaved function

$$T_a^n(x) := \int_0^x J_a^n(z) dz, \quad T_a^n(0) \equiv T_a^n(1) \equiv 0. \quad (18)$$

Integration of Eq. (17) yields the recursive functional equation

$$T_a^n(x) = t_a(x) + \frac{1}{m_a'(x)} T_a^{n-1}(m_a(x)) - I(x) \quad (19)$$

with the integral term

$$I(x) = \int_0^{m_a(x)} dz g_a''(z) T_a^{n-1}(z), \quad (20)$$

where $g_a''(z)$ is the second derivative of the inverse function of $m_a(x)$. The

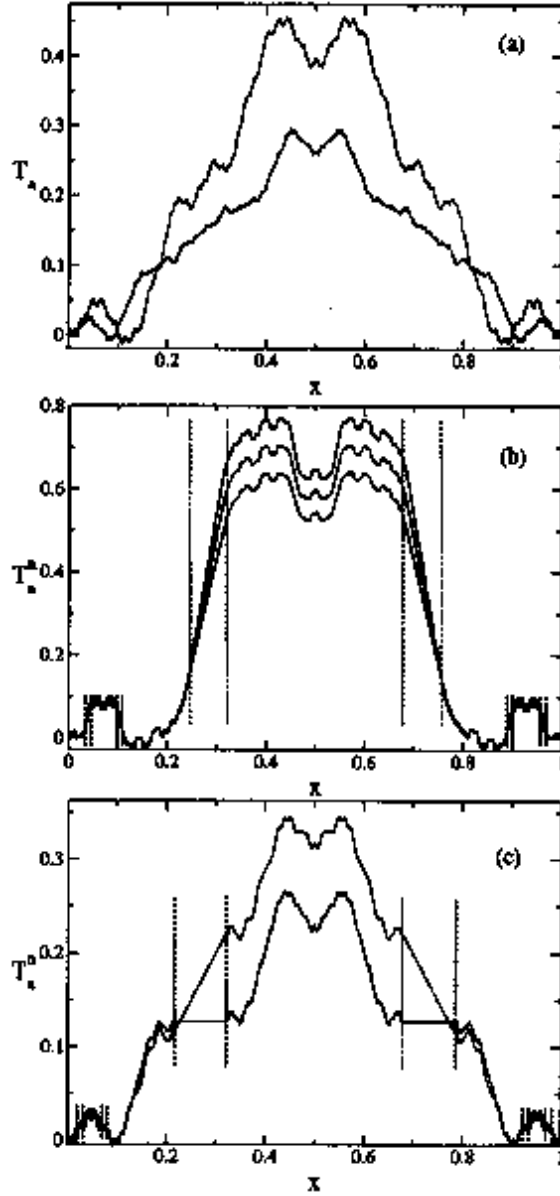


Fig. 7. (a): Generalized fractal Takagi functions for the diffusive climbing sine map with parameters $a = 1.2397$ (upper curve) and $a = 1.7427$ (lower curve). (b), (c): An example of nonconverging iterations of the generalized fractal Takagi functions for the climbing sine map with parameters corresponding to (b) ballistic dynamics at $a = 1.0$ and to (c) localized dynamics at $a = 1.5$, both for the time steps $n = 5, 6, 7$. Note the divergence of the iterations in (b) and the alternation between two states in (c).

function $t_a(x)$ is given by

$$t_a(x) = \int dz j_a(z) = x j_a(x) + c(x) , \quad (21)$$

where $c(x)$ is defined to be constant on each subinterval where the jump velocity $j_a(x)$ has a given value. This constant is fixed by the condition for $t_a(x)$ to be continuous on the unit interval supplemented by

$$t_a(0) = t_a(1) \equiv 0. \quad (22)$$

The generalized Takagi function is now defined in the long-time limit of Eq. (19),

$$T_a(x) = \lim_{n \rightarrow \infty} T_a^n(x). \quad (23)$$

For piecewise linear hyperbolic maps $I(x)$ in Eq. (20) simply disappears, and the derivative in front of the second term of Eq. (19) reduces to the local slope of the map thus recovering ordinary de Rham-type equations [3,4,38,41,42]. It should be noted that for smooth nonlinear maps like the climbing sine map the reduced map $m_a(x)$ is generally not invertible. In order to define a local inverse of $m_a(x)$, we split the unit interval into subintervals on which this function is piecewise invertible. Thus Eq. (19) should be understood as a series of equations where each part is defined for a respective piecewise invertible part of $m_a(x)$. The detailed derivation of Eq. (19) is given in Appendix B.

It is not known to us how to directly solve this generalized de Rham-type integro-differential equation for the climbing sine map, however, solutions can alternatively be constructed from Eqs. (18), (21), (22) starting from simulations. Results are shown in Fig. 7. For normal diffusive parameters the limit of Eq. (23) exists and the respective curves are fractal on the whole unit interval somewhat resembling standard Takagi functions [3,4,38,62,63]. However, in case of periodic windows $T_a^n(x)$ either diverges due to ballistic flights, or it oscillates indicating localization. Interestingly, in these functions the corresponding attracting sets appear in form of smooth, non-fractal regions on fine scales as marked by the dashed lines in Fig. 7.

The diffusion coefficient can now be formulated in terms of these fractal functions by carrying out the integrations contained in Eq. (10). For simplicity we restrict ourselves to the parameter region of $a \in (0.732644, 1.742726]$ in which the respective solution reads

$$D(a) = 2 [T_a(x_2)\rho(x_2) - T_a(x_1)\rho(x_1)] - D_0^\rho(a), \quad (24)$$

where x_i , $i = 1, 2$, is defined by $[M_a(x_i)] := 1$, and $D_0^\rho(a) := \int_{x_1}^{x_2} dx \rho(x)$. Our previous approximation $D_n^1(a)$ with $\rho(x) \simeq 1$ is recovered from this equation in form of

$$D_n^1(a) = 2 [T_a(x_2) - T_a(x_1)] - D_0^1(a). \quad (25)$$

Hence, Eqs. (24), (25) explicitly relate the generalized fractal Takagi functions shown in Fig. 7 to the fractals of Fig. 6.

6 Periodic windows

One of the most important problems regarding periodic windows in maps remains the question of their total measure. Much understanding has been achieved for one-dimensional unimodal maps [64,65,66,67,68,69,70]. Based on the Sharkovskii theorem about the ordering of periodic orbits [64], Metropolis, Stein and Stein organized periodic windows in universal symbolic sequences (U-sequences) such that the sequence of next order is uniquely determined by the previous one [65]. Later Jacobson came up with the proof that chaotic parameter values in one-dimensional unimodal maps with a single maximum do have positive measure [66]. Related numerical studies were made by Farmer [69]. Furthermore, it was shown that periodic windows in such a map form so-called fat fractal Cantor-like sets with positive measure.

However, for diffusive maps on a line, apart from the preliminary studies of Refs.[6,8], nothing appears to be known. On the other hand, as was exemplified in Sec. IV there is an intimate relation between the irregular structures of the diffusion coefficient and the occurrence of periodic windows. Hence, in this section we investigate the periodic windows for the climbing sine map in full detail.

Due to the spatial extension of our model a new type of periodic motion, which is not present in unimodal maps, exists, which is that particles move on average in one direction. These *ballistic solutions* are born through tangent bifurcations, further undergo a Feigenbaum-type scenario and die at crises points [6,8]. *Localized solutions* occur at even periods only and start with tangent bifurcations followed by a symmetry breaking at slope-type bifurcation points [6,8]. In this case the bifurcation scenario is much more complex. Obviously, periodic windows are related to certain periodic orbits, thus there are infinitely many of them, and they are believed to be dense in the parameter space [2].

By dividing the parameter line into subsets labeled by the integer value of the map maximum on the unit interval, $[M_a(X_{cr})] = j$, $j \in \mathbb{Z}$, we computed all windows of a certain period p in a certain subset. The numerical procedure which was used for these computations is outlined in Appendix C. Let T_j^p denote the total measure of all period p -windows in a subset j and let S_j^p be the partial sum of T_j^p defined by $S_j^p = \sum_{i=1}^p T_j^i$. In Fig. 8 $\log T_j^p$ is plotted as a function of the period for the three first subsets $j = 0, 1, 2$. The measures corresponding to windows with localized orbits are shown in Fig. 8 as pluses. Is it clear that they make the major contribution to the total measure for even periods hence explaining the origin of the pronounced oscillatory behavior of T_p^j .

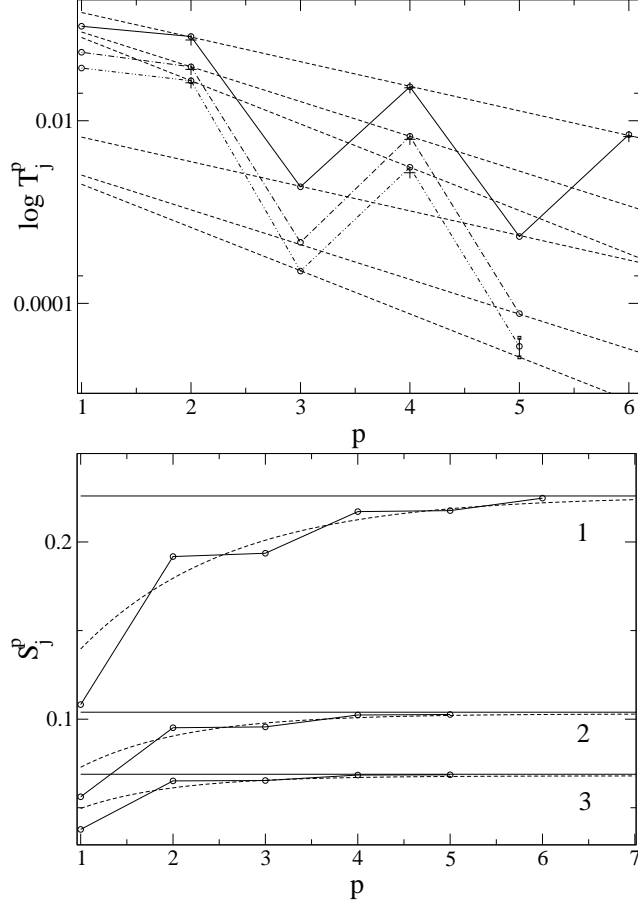


Fig. 8. Upper panel: The total measure T_j^p of all period p -windows (lines with symbols) for the first three parameter intervals (from top to bottom) as defined in the text. The dotted lines represent exponential fits; for the parameters see Table 1. The measures corresponding to windows with localized orbits are shown as pluses. Lower panel: The partial sum S_j^p for all periodic windows at a certain period p . The dashed curves represent approximations as calculated from Eq. (27), the straight lines are their limiting values at $p \rightarrow \infty$.

Table 1

Fit parameters for the exponential decrease of the measure at even and odd periods for the first three subsets of the map control parameter labeled by j .

j	a_j^{even}	b_j^{even}	a_j^{odd}	b_j^{odd}
0	0.284	0.61 ± 0.01	0.012	0.62
1	0.224	0.87 ± 0.01	0.007	0.89
2	0.242	1.01 ± 0.02	0.006	0.98

For odd periods all windows are due to ballistic orbits. Thus, we more carefully distinguish between even and odd periods. The dotted lines in Fig. 8 represent exponential fits to the functional dependence of the measure at even and odd periods according to $a_j^{even} \exp(-b_j^{even} p)$ and $a_j^{odd} \exp(-b_j^{odd} p)$, where j stands

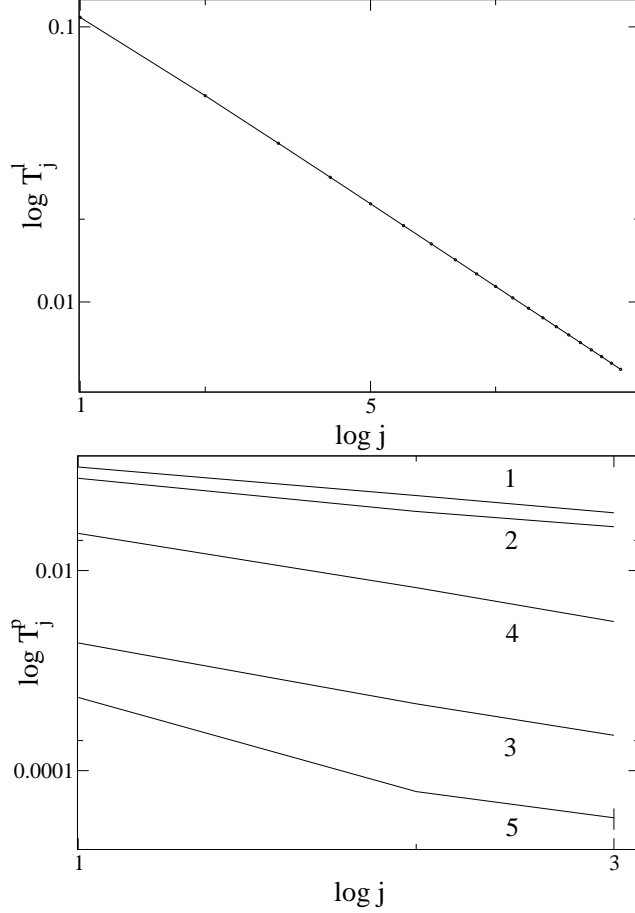


Fig. 9. Upper panel: Total measure T_j^1 for period one-windows as a function of the control parameter interval labeled by j . The slope of the line appears to be -1 (see text). Lower panel: the same as on the upper panel but here for different window periodicities p , and for smaller j . The labels at the single graphs give the value of p .

for the box number $j = 0, 1, 2$, as defined above. The fit parameters a_j, b_j are given in Table 1. From Fig. 8 and Table 1 one can conclude that the total measures at even and odd periods at a certain label j decrease approximately with the same rate, $b_j^{even} \sim b_j^{odd} \simeq b_j$. The exponential decrease of T_j^p suggests that the measure of chaotic solutions in each box, which is complementary to the measure of periodic windows, is indeed positive. Based on the information of T_j^p , it is straightforward to approximate the total measure of all the periodic windows in the j th box by

$$S_j = T_j^1 + \sum_{i=2}^{\infty'} T_j^i + \sum_{i=3}^{\infty''} T_j^i \simeq T_j^1 + \frac{a_j^{even} + a_j^{odd} e^{-b_j}}{e^{2b_j} - 1} \quad (26)$$

and to approximate the parameter dependence of the partial sum S_j^p to

$$S_j^p \simeq T_j^1 e^{-b_j(p-\frac{1}{2})} + S_j(1 - e^{-b_j(p-\frac{1}{2})}). \quad (27)$$

Table 2

The Lebesgue measure Δ_j , the total measure of periodic windows S_j , and the complementary measure of chaotic solutions C_j for the first three subsets of the map control parameter labeled by j .

j	Δ_j	S_j	C_j
0	1.01008	0.226 ± 0.002	0.783 ± 0.002
1	1.00265	0.103 ± 0.002	0.898 ± 0.002
2	1.00123	0.068 ± 0.002	0.932 ± 0.002

Sums with one or two primes go only over even or odd terms, respectively. In the lower panel of Fig. 8 results for S_j are shown as horizontal lines, the dashed lines in the upper panel (without symbols) are the approximations for S_j^p according to Eq. (27).

The values for the measure of all periodic windows in the j th box, S_j , and the measure of the chaotic solutions $C_j = \Delta_j - S_j$, where Δ_j is the total measure of the j box, are listed in Table 2 for the first three subsets of the control parameter.

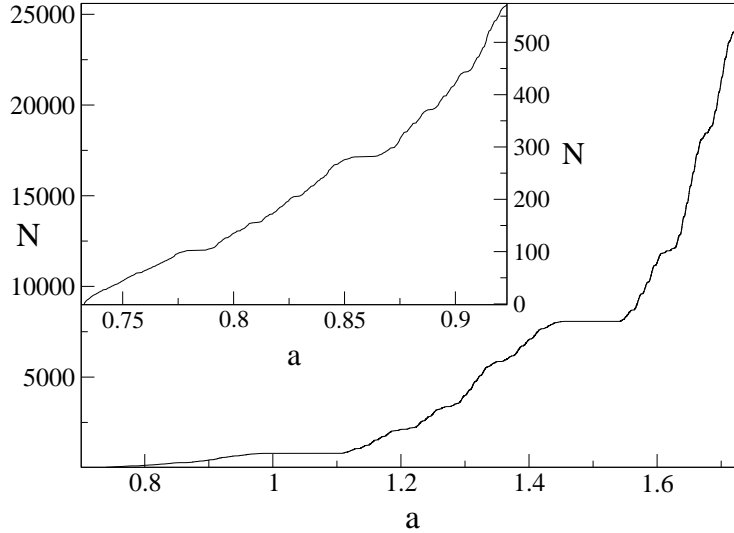


Fig. 10. Devil's staircase like structure formed by the distribution of periodic windows as a function of the control parameter. N is the integrated number of period six-windows. The inset shows a blowup of the initial region.

The main message of Table 2 is that the measure of periodic windows is different for a different subset j and obviously decreases by increasing the control parameter. Correspondingly, the measure of chaotic solutions increases as the parameter of the system is getting larger. In order to make this more quantitative we consider the dependence of the measure of period p -windows as a function of the box index j . First we check period one-windows. Since in each box there exists only one window of this period, we are able to go to up

to $j = 20$. In the upper panel of Fig. 9 the logarithm of T_j^1 is plotted against $\log j$. We find that the slope of this function almost exactly equal to -1 . The behavior of T_j^p for different p is shown in the lower panel of Fig. 9. The slope of the line for period two is also -1 , for period three and four it is -2 , and for period five it is -3 . Fig. 9 shows that even and odd periods decrease with respectively different laws, where the decay rate appears to be precisely given by the periodicity of the windows according to $1/j^{p/2}$ for even periods and $1/j^{(p+1)/2}$ for odd periods.

In order to analyze the structure of the regions of anomalous diffusion in the parameter space, we sum up the number of period six-windows as a function of the parameter, that is, the total number is increased by one for any parameter value at which a new period six-window appears. This sum forms a Devil's staircase like structure in parameter space indicating an underlying Cantor set like distribution for the corresponding anomalous diffusive region, see Fig. 9. Since the Lebesgue measure of periodic windows is positive, this set must be a fat fractal [68]. Its self-similar structure can quantitatively be assessed by computing the so-called fatness exponent. Following [69], let $h(\varepsilon)$ be the total measure of all periodic windows whose width is greater than or equal to ε . Define the coarse-grained measure as $\mu(\varepsilon) = \Delta - h(\varepsilon)$, where Δ is the total measure of a box related to the control parameter. For quadratic maps on the interval, it was conjectured and confirmed numerically that $\mu(\varepsilon)$ asymptotically scales as a power law in the limit of $\varepsilon \rightarrow 0$,

$$\mu(\varepsilon) \approx \mu(0) + A\varepsilon^\beta, \quad (28)$$

where $\mu(0)$ is the measure of chaotic parameters. β was called the fatness exponent. For quadratic maps it was found to be $\beta \simeq 0.45$. Since our map belongs to the same universality class as considered in Farmer's case, namely the map has a single quadratic maximum, one may expect that β will have the same value. For the climbing sine map a double-logarithmic plot of $\delta\mu(\varepsilon) = \mu(\varepsilon) - \mu(0)$ is shown in Fig. 11 for the first three boxes, $j = 0, 1, 2$. In all cases the bold lines have the slope 0.45 with errors of 0.03, 0.04, 0.05, respectively, which seems to be in agreement with Farmer's conjecture about the universality of β . However, apart from this coarse linear behavior one can see an interesting oscillatory behavior in $\delta\mu$ with respect to ε . This fine structure can be explained with respect to the histogram distribution functions f of the window sizes d , which are plotted in Fig. 11 in form of dashed lines. Somewhat surprisingly, the periodic windows are not distributed uniformly or smoothly with respect to their size but form certain peaks, in which preferably windows of certain periods are grouped together. This non-uniformity is clearly reflected in the oscillations of $\delta\mu(\varepsilon)$. Moreover, we find that the size distributions of periodic windows have a fine structure that appears to resemble a fractal function. Some evidence for this property is given in the inset of Fig. 11 (c), which shows the size of every window of period five in the subset $j = 2$ as a function of its appearance with respect to the map control parameter a , i.e., not the parameter itself

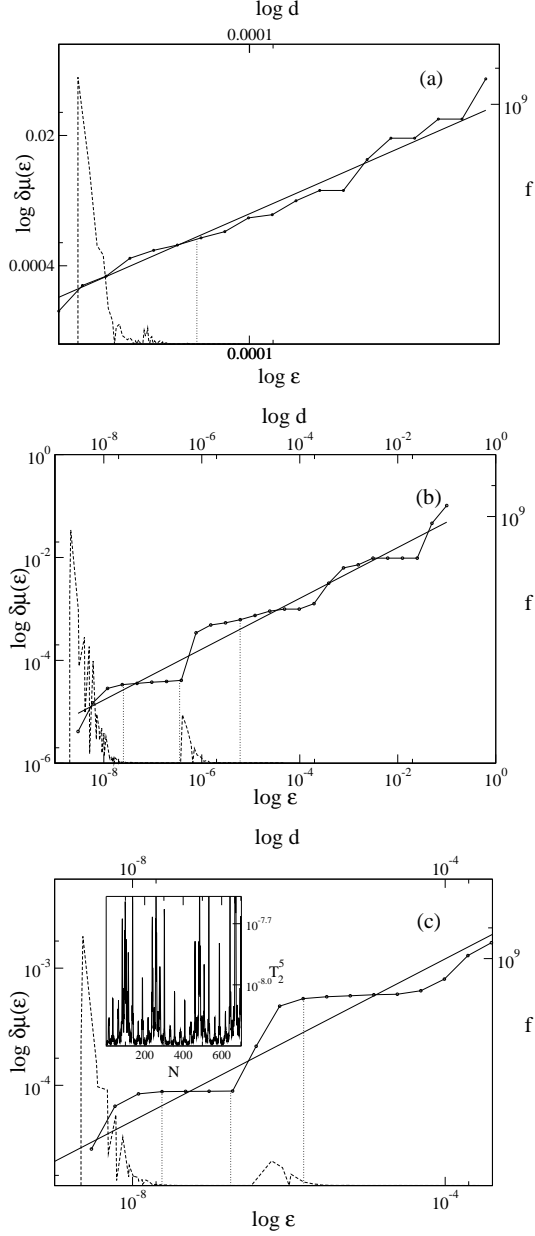


Fig. 11. Difference $\delta\mu = \mu(\varepsilon) - \mu(0)$, where $\mu(\varepsilon)$ is the total measure of windows that are smaller than ε . Results are plotted for the first three subsets $j = 0, 1, 2$ of the map control parameter, from top to bottom. In all cases, the slope of the solid lines is approximately 0.45. The dashed lines in each graph represent the corresponding coarse-grained window distribution functions. In the inset of Fig. (c) the measure of any single period five-window in the subset $j = 2$ is shown with respect to an integer label that accounts for the ordering according to the map control parameter.

is plotted but just an integer running index N is given instead. Particularly the height of the peaks is important, and one can clearly see a complicated hierarchy of different peaks which are reminiscent of the fine structure in the corresponding distribution function shown in Fig. 11 (c).

7 Conclusions

In this paper we have performed a detailed analysis of the parameter dependence of the diffusion coefficient in a nonhyperbolic dynamical system. The climbing sine map has been chosen as a paradigmatic example of such a system. We have shown that, on a coarse scale, there are certain analogies between the parameter-dependent diffusion coefficient of this map and the ones in simple hyperbolic piecewise linear maps, such as the existence of an oscillatory structure, and the existence of asymptotic functional forms as derived from simple random walk models. However, in contrast to hyperbolic maps showing normal diffusion only, in the nonhyperbolic climbing sine map fractal structures appear for both normal and anomalous diffusive regions of the diffusion coefficient. An understanding of the origin of these fractal structures was given in terms of dynamical correlations starting from the Green-Kubo formula for diffusion. We furthermore related these irregularities in the diffusion coefficient more microscopically to different characteristics in corresponding fractal generalized Takagi functions. For this purpose we derived a new functional recursion relation that defines these fractal forms and generalizes ordinary de Rham-type equations. Our analysis was completed by extensive numerical studies of the periodic windows of the climbing sine map showing that both the periodic and the chaotic parameter regions have positive measures in the parameter space. However, these measures are themselves parameter-dependent, and by increasing the parameter we found that the chaotic regions occupy larger and larger measures. We finally provided evidence that these different sets form fat fractals on the parameter axis.

In conclusion, we wish to remark that the climbing sine map is of the same functional form as the respective nonlinear equation in the two-dimensional standard map, which is considered to be a standard model for many physical Hamiltonian dynamical systems. Indeed, both models are motivated by the driven nonlinear pendulum, both are strongly nonhyperbolic, and though the standard map is area-preserving it too exhibits a highly irregular parameter-dependent diffusion coefficient. Understanding the origin of these irregularities was the subject of intensive research [2,19], however, so far the complexity of this system did not enable to reveal its possibly fractal nature. A suitably adapted version of our approach to nonhyperbolic diffusive dynamics as presented in this paper may enable to make some progress in this direction.

Another interesting problem is to possibly further exploit the concept of conjugacy between nonlinear and piecewise linear maps, as explained in Sec. III, in order to exactly calculate diffusion coefficients for nonlinear maps. A very promising approach in this direction was presented in Ref. [56]. Based on these techniques we are planning to perform a spectral analysis of the Frobenius-Perron operator governing the probability density of the diffusive climbing sine

map. Combining such an analysis with the Takagi function approach outlined here may lead to a general theory of nonhyperbolic transport.

It would furthermore be important to check out the applicability of periodic orbit theory for computing the parameter-dependent diffusion coefficient of the climbing sine map, which may provide an alternative method [15]. Another promising direction of future research concerns establishing crosslinks between our work and the realm of strange kinetics and stochastic modeling as described in Refs. [24,25,26], e.g., by trying to apply continuous time random walk techniques to more complicated chaotic models exhibiting fractal diffusion coefficients such as the climbing sine map.

We finally emphasize the importance to look for possibly fractal transport coefficients in experiments. A very promising candidate appears to be the phase dynamics in SQUID's, which was very recently analyzed theoretically [48] and studied experimentally [49].

A Diffusion coefficients of two conjugate maps

In this Appendix we give a proof of the statement of Grossmann and Thomae [9] that two diffusive maps which are conjugate to each other have the same diffusion coefficient.

Two diffusive maps $F : I \rightarrow I$ and $G : J \rightarrow J$ are called conjugate [58,9,55] if there exists a map $H : I \rightarrow J$ such that $F(x) = H(G(H^{-1}(x)))$. Let us assume in the following that the conjugation function H is sufficiently smooth. Let the invariant densities of the corresponding reduced (*mod* 1) maps be $\tilde{\rho}(x)$ for $F(x) \bmod 1$ and $\rho(y)$ for $G(y) \bmod 1$; then it is, according to conservation of probability, $\tilde{\rho}(x) = |(H^{-1}(x))'| \rho(H^{-1}(x))$. The diffusion coefficients of the maps $F(x)$ and $G(y)$ we denote by D_F and D_G , respectively. Without loss of generality let us furthermore assume that the maxima of both maps are in the interval $[1, 2]$.

We now start with the Green-Kubo formula written in *correlated random walk* terms as

$$D_F = \frac{1}{2} \int_0^1 [F(x)]^2 \tilde{\rho}(x) dx + \int_0^1 [F(x)] \cdot B(x) \tilde{\rho}(x) dx, \quad (\text{A.1})$$

where

$$B(x) = [F\{F(x)\}] + \dots + [F(\{F(\{\dots(\{F(x)\})\dots\})\})] + \dots, \quad (\text{A.2})$$

or shortly

$$D_F = d_{F_0} + d_{F_1} + d_{F_2} + \dots \quad (\text{A.3})$$

where

$$d_{F_0} = \frac{1}{2} \int_0^1 [F(x)]^2 \tilde{\rho}(x) dx, \quad (\text{A.4})$$

$$d_{F_1} = \frac{1}{2} \int_0^1 [F(x)] [F\{F(x)\}] \tilde{\rho}(x) dx, \quad (\text{A.5})$$

and so on. Focusing on the first term, one can rewrite this expression using the symmetry of the map to

$$d_{F_0} = \frac{1}{2} \int_0^1 [F(x)]^2 \tilde{\rho}(x) dx = \int_{x_1}^{x_2} \tilde{\rho}(x) dx, \quad (\text{A.6})$$

where x_1, x_2 defines an escape region. For the conjugate map $G(y)$ the respective term reads

$$d_{G_0} = \frac{1}{2} \int_0^1 [G(y)]^2 \rho(y) dy = \int_{y_1}^{y_2} \rho(y) dy, \quad (\text{A.7})$$

where y_1, y_2 is the corresponding escape region for G . Note that the escape regions (x_1, x_2) and (y_1, y_2) are not the same, however, it is straightforward to show that $H(x_i) = y_i$, $i = 1, 2$, that is, the topology of both maps is conserved such that the two escape regions are mapped onto each other under conjugacy.

Taking into account the conservation of probability mentioned before one immediately gets

$$d_{F_0} = d_{G_0}. \quad (\text{A.8})$$

All other terms d_{F_1}, d_{F_2}, \dots and d_{G_1}, d_{G_2}, \dots have the form

$$d_{(F,G)_i} = A \int_{\delta_{esc}} \nu(z) dz, \quad i = 1, 2, \dots \quad (\text{A.9})$$

where A is a constant, δ_{esc} is the respective escape region and $\nu(z) dz$ is the corresponding invariant measure. Thus, the same argument can be applied to show that $d_{F_i} = d_{G_i}$, ($i = 1, 2, \dots$). Combining all results we arrive at

$$D_F = D_G. \quad (\text{A.10})$$

B Recursion relation for generalized Takagi functions

We start with the recursion relation for the jump velocity function Eq. (17),

$$J_a^n(x) = j_a(x) + J_a^{n-1}(m_a(x)), \quad (\text{B.1})$$

by recalling the definition of the generalized Takagi function Eq. (18),

$$T_a^n(x) := \int_0^x J_a^n(z) dz, \quad T_a^n(0) \equiv T_a^n(1) \equiv 0, \quad (\text{B.2})$$

or differently

$$J_a^n(x) = \frac{d}{dx} T_a^n(x). \quad (\text{B.3})$$

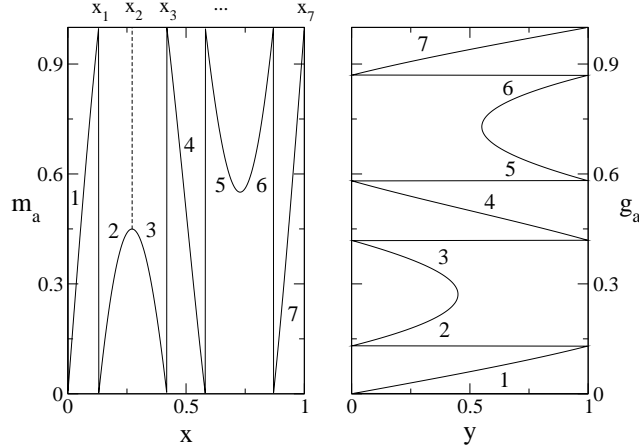


Fig. B.1. Illustration of the construction of the inverse function of the climbing sine map for the parameter value $a = 1.189$. Piecewise invertible branches are labeled by the integer numbers $i = 1, \dots, 7$.

We have to integrate Eq. (B.1),

$$\int_0^x dy J_a^n(y) = \int_0^x dy j_a(y) + \int_0^x dy J_a^{n-1}(m_a(x)). \quad (\text{B.4})$$

By using of Eq. (B.2) we get

$$T_a^n(x) = t_a(x) + I(x), \quad x \in (0, 1], \quad (\text{B.5})$$

where

$$I(x) = \int_0^x dy J_a^{n-1}(m_a(y)), \quad x \in (0, 1]. \quad (\text{B.6})$$

Without loss of generality let us assume that the maximum of the map is in the interval $[1, 2]$.

Depending on x the integral in Eq. (B.6) can be decomposed into

$$I_1(x) = \int_0^x dy J_a^{n-1}(m_a(y)), \quad x \in (0, x_1]; \quad (\text{B.7})$$

$$I_2(x) = \int_0^{x_1} dy J_a^{n-1}(m_a(y)) + \int_{x_1}^x dy J_a^{n-1}(m_a(y)), \quad x \in (x_1, x_2];$$

$$I_3(x) = \dots, \quad x \in (x_2, x_3]; \quad \dots \quad I_6(x) = \dots, \quad x \in (x_5, x_6];$$

$$I_7(x) = \int_0^{x_1} dy J_a^{n-1}(m_a(y)) + \dots + \int_{x_6}^x dy J_a^{n-1}(m_a(y)), \quad x \in (x_6, x_7].$$

Each integral in Eq. (B.7) now contains only one piecewise invertible branch of the reduced map $m_a^i(x)$ as shown in Fig. B.1. Here, the piecewise invertible branches of the reduced map are labeled by integers, and the corresponding branches of the inverse function $g_a^i(y)$ have the same indices $i = 1, \dots, 7$. Since all integrals in Eq. (B.7) have the same form (only the inverse parts of the reduced map are different), we restrict ourselves to the integral

$$I(x) = \int_0^x dy J_a^{n-1}(m_a^i(y)). \quad (\text{B.8})$$

Making the change of variables $z = m_a^i(y)$ and using the definition of the generalized Takagi function Eq. (B.3) we get

$$I(x) = \int_0^{m_a^i(x)} dz (g_a^i(z))' \frac{d}{dz} T_a^{n-1}(z). \quad (\text{B.9})$$

Using integration by parts we arrive at

$$I(x) = (g_a^i(z))' \cdot T_a^{n-1}(z) \Big|_0^{m_a^i(x)} - \int_0^{m_a^i(x)} dz (g_a^i(z))'' \cdot T_a^{n-1}(z). \quad (\text{B.10})$$

Now recall that according to Eq. (B.2) it is $T_a^{n-1}(m_a^i(x_j)) \equiv 0$, where the x_j define the boundaries of the piecewise invertible parts of $m_a(x)$, see Fig. B.1, and that $(g_a^i(z))' \Big|_{z=m_a^i(x)} \equiv 1/(m_a^i(x))'$. Thus, by formally defining the inverse function $g_a(x)$ as consisting of all branches $i = 1, \dots, 7$, we can finally write Eq. (B.5) in the form

$$T_a^n(x) = t_a(x) + \frac{1}{m_a'(x)} T_a^{n-1}(m_a(x)) - I(x) \quad (\text{B.11})$$

with the integral term

$$I(x) = \int_0^{m_a(x)} dz g_a''(z) T_a^{n-1}(z). \quad (\text{B.12})$$

C Numerical procedure for calculating the measure of the periodic windows

The parameter values a_{tan} which correspond to the tangent bifurcations of the p -periodic windows were found by solving the two coupled transcendental equations

$$\partial m_{a_{tan}}^{(p)}(x)/\partial x = 1, \quad m_{a_{tan}}^{(p)}(x) - x = 0, \quad (\text{C.1})$$

where $m_a^{(p)}(x)$ denotes the p -times iterated reduced map. This corresponds to the situation where $m_a^{(p)}(x)$ touches the bisector. Somewhat after a tangent bifurcation one will unavoidably find a situation where a critical point x_c , which corresponds to an extremum of $m_a^{(p)}(x)$, crosses the bisector. When this critical point is exactly located on the diagonal, the reduced map or its higher iterations have a fixed point and there exists a specific Markov partition on the interval [37,38]. The periodic orbit generated by the corresponding parameter value a_{ss} is superstable,

$$m_{a_{ss}}^{(p)}(x_c) - x_c = 0. \quad (\text{C.2})$$

By further increasing the parameter value up to a_{cr} a crisis takes place, and this again corresponds to the existence of a certain Markov partition.

Based on this scenario, the full numerical procedure which was used for calculating the measure of periodic windows is as follows: The values of a_{ss} corresponding to superstable solutions were first calculated by a combination of bisection with the Newton method. The parameters for the tangent bifurcations could then usually be found by the modified two-dimensional Newton method [69]. However, the highly discontinuous nature of $m_a^{(p)}(x)$ made its implementation very inefficient. Instead, starting in the vicinity of each a_{ss} we again combined the one-dimensional Newton and bisection methods. This ensured that no windows were missed. Finally, the parameter values corresponding to crisis points a_{cr} , which are also defined by Markov partitions, can be found by solving respective equations that are formally analogous to Eq. (C.2).

References

- [1] A. Lichtenberg and M. Lieberman, Regular and Stochastic Motion, Springer, New York, 1983.

- [2] E. Ott, Chaos in dynamical systems, Cambridge University Press, Cambridge, England, 1997.
- [3] P. Gaspard, Chaos, Schattering and Statistical Mechanics, Cambridge University Press, Cambridge, England, 1998.
- [4] J.R. Dorfman, An Introduction to Chaos in Non-Equilibrium Statistical Mechanics, Cambridge University Press, Cambridge, England, 1999.
- [5] T. Geisel, J. Nierwetberg, Phys. Rev. Lett. **48**, 7 (1982).
- [6] M. Schell, S. Fraser, R. Kapral, Phys. Rev. A **26**, 504 (1982).
- [7] S. Grossmann and H. Fujisaka, Phys. Rev. A **26**, 1779 (1982).
- [8] H. Fujisaka and S. Grossmann, Z.Phys.B - Condensed Matter **48**, 261 (1982).
- [9] S. Grossmann and S. Thomae, Phys. Lett. **97A**, 263 (1983).
- [10] L.Sh. Tsimring, Physica D **63**, 41 (1993).
- [11] P. Reimann, Phys. Rev. E **50**, 727 (1994).
- [12] I. Dana and M. Amit, Phys. Rev. E **51**, R2731 (1995).
- [13] S. Prakash, C.-K. Peng and P. Alstøm, Phys. Lett. A **43**, 6564 (1991).
- [14] B.V. Chirikov and V.V. Vecheslavov, nlin.CD/0202017.
- [15] P. Cvitanović, R. Artuso, R. Mainieri, G. Tanner and G. Vattay, *Classical and Quantum Chaos*, www.nbi.dk/ChaosBook/, Niels Bohr Institute (Copenhagen 2001)
- [16] R. Artuso, Phys. Lett. A **160**, 528 (1991).
- [17] H.-C. Tseng, H.-J. Chen, P.-C. Li, W.-Y. Lai, C.H. Chou, H.-W. Chen, Phys. Lett. A **21**, (1994), 74.
- [18] Ch.-Ch.. Chen, Phys. Rev. E **51**, 2815-2822 (1995).
- [19] A.B. Rechester, R.B. White, Phys. Rev. Lett. **44**, 1586 (1980).
- [20] A.B. Rechester, M.N. Rosenbluth, R.B. White, Phys. Rev. A **23**, 2664 (1981).
- [21] R. Ishizaki, *et al.* Prog. Theor. Phys. **85**, 1013 (1991).
- [22] G.M. Zaslavsky, M. Edelman, and B.A. Niyazov, Chaos **7**(1), 159 (1997).
- [23] P. Leboeuf, Physica **116D**, 8 (1998).
- [24] G. Zumofen, J. Klafter, Phys. Rev. E **47**, 851 (1993).
- [25] J. Klafter and G. Zumofen, Phys. Rev. E **49**, 4873 (1994); *ibid.* **51**, 1818 (1995).
- [26] R. Metzler, J. Klafter, Phys. Rep. **339**, 1 (2000).
- [27] T. Harayama and P. Gaspard, Phys. Rev. E **64**, 036215.

- [28] R. Klages and C. Dellago, *J. Stat. Phys.* **101**, 145 (2000).
- [29] R. Klages, and N. Korabel *J. Phys. A: Math. Gen.* **35**, 4823 (2002).
- [30] B.V. Chirikov, *Phys. Rep.* **52**, 263 (1979).
- [31] B.A. Huberman, J.P. Crutchfield, and N.H. Packard, *Appl. Phys. Lett.* **37**(8), 750 (1980).
- [32] N.F. Pedersen and A. Davidson, *Appl. Phys. Lett.* **39**(10), 830 (1981).
- [33] R.F. Miracky, M.H. Devoret, and J. Clarke, *Phys. Rev. A* **31**, 2509 (1985).
- [34] J.A. Blackburn, N. Grønbech-Jensen, *Phys. Rev. E* **53**, 3068 (1996).
- [35] R. Festa, A. Mazzino, and D. Vincenzi, *nlin.CD/0204020*.
- [36] H. Sakaguchi, *Phys. Rev. E* **65**, 067201.
- [37] R. Klages, and J.R. Dorfman, *Phys. Rev. Lett.* **74**, 387 (1995).
- [38] R. Klages, *Deterministic Diffusion in One-Dimensional Chaotic Dynamical Systems* (Wissenschaft & Technik Verlag, Berlin, 1996).
- [39] R. Klages, and J.R. Dorfman, *Phys. Rev. E* **55**, R1247 (1997).
- [40] R. Klages, and J.R. Dorfman, *Phys. Rev. E* **59**, 5361 (1999).
- [41] P. Gaspard and R. Klages, *Chaos* **8**, 409 (1998).
- [42] J. Groeneveld and R. Klages, *J. Stat. Phys.* **109**, 821 (2002).
- [43] V.N. Belykh, N.F. Pedersen, and O.H. Soerensen, *Phys. Rev. B* **16**, 4860 (1977).
- [44] E. Ben-Jacob *et al.*, *Appl. Phys. Lett.* **38**(10), 822 (1981).
- [45] M. Cirillo and N.F. Pedersen, *Phys. Lett.* **90A**, 150 (1982).
- [46] R.F. Miracky, J. Clarke, and R.H. Koch, *Phys. Rev. Lett.* **11**, 856 (1983).
- [47] J.M. Martinis and R.L. Kautz, *Phys. Rev. Lett.* **63**, 1507 (1989).
- [48] K.I. Tanimoto, T. Kato, and K. Nakamura, *Phys. Rev. B* **66**, 012507 (2002).
- [49] S. Weiss *et al.*, *Europhys. Lett.* **51**, 499 (2000).
- [50] H.U. Beyeler, *Phys. Rev. Lett.* **37**, 1557 (1976).
- [51] S. Martin and W. Martienssen, *Phys. Rev. Lett.* **56**, 1522 (1986).
- [52] S.E. Brown, G. Mozurkewich, and G. Gruener, *Phys. Rev. Lett.* **52**, 2277 (1984).
- [53] H. Koga, H. Fujisaka, and M. Inoue, *Phys. Rev. A* **28**, 2370 (1983).
- [54] T. Bohr, P. Bak, M.H. Jensen, *Phys. Rev. A* **30**, 1970 (1984).
- [55] A. Lasota and M.C. MacKey, *Chaos, Fractals, and Noise*. Springer-Verlag, New York, 1994.

- [56] D. Alonso, D. MacKernan, P. Gaspard, G. Nicolis, *Phys. Rev. E* **54**, 2474 (1996).
- [57] S. Tasaki, private communications.
- [58] S. Grossmann and H. Fujisaka, *Z.Naturforsch.* **32a**, 1353 (1977).
- [59] T. Takagi, *The Collected papers of Teiji Takagi* (Iwanami Shoten Pub., 1973, 5-6).
- [60] G. de Rham, *Enseign. Math.* **3**, 71 (1957).
- [61] M. Hata and M. Yamaguti, *Japan J. Appl. Math.* **1**, 183 (1984).
- [62] S. Tasaki, I. Antoniou and Z. Suchanecki, *Phys. Lett. A* **179**, 97 (1993).
- [63] P. Gaspard, *Int. J. of Mod. Phys. B* **15** (3), 209 (2001).
- [64] A.N. Sharkovskii, *Ukr. Mat. Z.* **16**, 61 (1964).
- [65] N. Metropolis, M.L. Stein, and P.R. Stein, *J. Combin. Theor.* **15**, 25 (1973); and references therein.
- [66] M.V. Jacobson, *Soviet. Math. Dokl.* **19**, 1452 (1978).
- [67] M.J. Feigenbaum, *J. Stat. Phys.* **19**, 25 (1979), and **21**, 669 (1979); *Physica* **7D**, 16 (1983).
- [68] J.A. Yorke *et al.*, *Phys. Rev. Lett.* **54**, 1095 (1985).
- [69] J.D. Farmer, *Phys. Rev. Lett.* **55**, 351 (1985).
- [70] C. Grebogi and E. Ott, and J.A. Yorke, *Physica* **7D**, 181 (1983).